10-3-2018

# Simulating the Role of Axial Flow in Stay Cable Vibrations via a Perforated Wake Splitter Plate", ASCE Special Edition: Wind Engineering in Natural Hazards

Ran Wang
*University of Windsor*

Shaohong Cheng
*University of Windsor*

David S-K Ting
*windsor*

# Simulating the Role of Axial Flow in Stay Cable Vibrations via a Perforated Wake Splitter Plate

Ran Wang [a], Shaohong Cheng[b,1], David S-K. Ting[c]

[a,b]Department of Civil and Environmental Engineering, University of Windsor
[c]Department of Mechanical, Automotive and Materials Engineering, University of Windsor
401 Sunset Avenue, Windsor, Ontario, Canada, N9B 3P4
[a]wang1hf@uwindsor.ca, [b]shaohong@uwindsor.ca, [c]dting@uwindsor.ca

**Abstract:** The inclined and/or yawed orientation of bridge stay cables results in the formation of secondary axial flow on the leeward side of cable surface, which is believed to be one of the contributing factors exciting some unique wind-induced cable vibration phenomena. To clarify the role of axial flow in triggering aerodynamic instability of stay cables, a numerical study has been conducted to indirectly examine the axial flow effect via a perforated splitter plate placed along the central line of a circular cylinder wake. By manipulating the perforation ratio of the perforated plate at four different levels, the variation of von Kármán vortex shedding strength, which reflects the axial flow intensity, can be simulated. The impact of the splitter plate perforation ratio on the flow structure around a circular cylinder, in terms of the instantaneous vortex structure, the surface pressure distribution and the aerodynamic forces are discussed in detail by exploiting the numerical data obtained from the large eddy simulation. Results show that the presence of a perforated wake splitter plate would play a similar role as the axial flow in affecting the strength of von Kármán vortex shedding. A more solid wake splitter plate is found to cause a stronger interruption on the interaction between the shear layers formed on the two sides of the cylinder and consequently lead to a more symmetric surface pressure distribution pattern and weaker von Kármán vortex shedding strength. Reductions on the fluctuating amplitude of the instantaneous lift and drag as well as the mean drag are also observed, which would ultimately affect the aerodynamic response of the studied cylinder.

[1] Corresponding author, Tel.: +15192533000, ext. 2629, fax:+5199713686
Email address: shaohong@uwindsor.ca

**Keywords:** circular cylinder; perforated wake splitter plate; von Kármán vortex shedding; axial flow; cable vibrations; cable-stayed bridges; aerodynamic instability; large eddy simulation

## 1. INTRODUCTION

Cable-stayed bridges have become progressively popular since the completion of the Stromsund Bridge in Sweden in 1955, mainly due to their modest requirement on ground anchorage condition, efficient utilization of structural material, higher stiffness and economy compared to the suspension bridges. Rapid development in materials, design and construction technology constantly push the bridge span to a new limit. Currently, the record holder of the cable-stayed bridge, the Russky Bridge in Russia, has a center span length of 1104 m and the longest cable on the bridge is 580 m. The road deck of the highest cable-stayed bridge, the Duge bridge in China inaugurated in 2016, sits over 565 m above the Beipan river. These great advancements are, naturally, accompanied with new engineering challenges. Owing to the low lateral stiffness, low inherent damping and small mass, stay cables on cable-stayed bridges are prone to dynamic excitations. Further, the inclined and/or yawed orientation of stay cables against the oncoming wind introduces some unique wind-induced cable vibration phenomena, the mechanisms of which are yet to be fully comprehended.

Excessive vibrations of cables on cable-stayed bridges have been frequently reported in recent years. Among these incidents, rain-wind-induced vibration (RWIV) is observed most on site. This sort of vibration was first reported by Hikami and Shiraishi (1988) on the Meiko-Nishi bridge in Japan. After that, numerous similar cases were reported (Stafford and Watson, 1988; Pacheco, 1993; Persoon and Noorlander, 1999; Main and Jones, 2000; Matsumoto et al. 2003; Zuo et al. 2008; Zuo and Jones, 2010). Extensive researches have been conducted to unveil the mystery, mainly using wind tunnel tests (Matsumoto et al., 1992; 1995; Flamand, 1995; Bosdogianni and Olivari, 1996; Ming, 2002; Gu and Du, 2005; Alam and Zhou, 2007;

Li et al., 2016; Jing et al., 2017), theoretical (Yamaguchi, 1990; Gu and Lu, 2001; Cao et al., 2003; He et al., 2010; 2012; Li et al., 2013) and numerical analyses (Seidel and Dinkler, 2006; Robertson et al., 2010; Li et al., 2010; Bi et al., 2013; Wang et al., 2016). While many studies have been carried out to investigate the excitation mechanisms of RWIVs, researchers held different or even conflicting ideas and no consensus has been reached so far (Jing et al., 2017b). Nevertheless, the formation of upper water rivulet on the cable surface is considered to be an important factor to induce RWIV.

Dry inclined cable galloping has been proved theoretically to be a potential safety threat to bridge stay cables (Piccardo, 1993; Macdonald and Larose, 2008; Raeesi et al., 2014; He and Macdonald, 2016). Saito et al. (1994) proposed an instability criterion which suggested that the onset condition of dry inclined cable galloping could be easily satisfied for many stay cables on existing bridges and the unstable cable motion could not be suppressed by introducing additional damping. However, this criterion is too conservative to be applied to bridge design and field experience indicated that this was not the case. Outcomes of earlier studies indicated that the necessary conditions to trigger dry inclined cable galloping would include: a) emergence of critical Reynolds number regime (Macdonald and Larose, 2006; Cheng et al., 2008a; 2008b); b) presence of axial flow (Matsumoto et al., 1992; 1995; 2003; 2005); and c) sustained duration of the critical flow condition (Raeesi et al., 2014). Also, high span-wise correlation of aerodynamic forces on the cable upon the onset of dry galloping was found by Cheng and Tanaka (2005). It is worth noting that, up till now, no field incident of dry inclined cable galloping has been formally confirmed, despite a few wind tunnel tests (Miyata et al., 1994; Cheng et al., 2003; 2008b)Jakobsen et al., 2012; Vo et al., 2016) observed the occurrence of this type of instability. reported both divergent and limited-amplitude cable vibrations at high reduced wind speed. Zuo and Jones (2009) suspected that the dry galloping observed in the wind tunnel test by Cheng et al. (2003; 2008a) might relate to rain-wind-

induced vibration in the field. However, it is challenging in acquiring accurate onsite environment data at the occurrence of violent cable vibrations, such as the particular amount of precipitation, wind speed and direction. The possible existence of the so-called “rain-wind-induced vibration” in the absence of rainfall, and the possible relation between the vibrations observed on wet and dry cables is still unclear.

A circular cylinder in cross-flow has been extensively studied both experimentally and numerically. However, in the case of a bridge stay cable, though it is typically modeled as a circular cylinder in existing studies, the flow structure around it is much more complex due to its inclined and yawed orientation. This renders the formation of the secondary axial flow on the leeward side of the cable surface which disturbs the interaction between the shear layers separated from the two sides of the cylinder and suppresses the shedding of the von Kármán vortices. Shirakashi et al. (1986) investigated the aerodynamic behaviour of a yawed circular cylinder in uniform flow in the wind tunnel and concluded that the reduction of the vortex shedding frequency by yawing was attributed to the presence of the secondary flow behind the cylinder. Matsumoto et al. (1990) reported that depending on the boundary condition, the intensity of the axial flow formed on the leeward side of a circular cylinder yawed at $45^{\circ}$ varied between 40% to 60% of the oncoming flow velocity.

From the existing studies, it is understood that a splitter plate could be used as a passive device to control the vortex formation in the wake of a cylinder (Roshko and Anato, 1954; Apelt et al., 1973; Apelt and West, 1975; Ozono, 1999; Choi, 2007; Dehkordi and Jafari, 2010; Ali et al., 2012). Therefore, it is expected that a wake splitter plate would play a similar role as that of the axial flow in interrupting the communications between separated flow from the two sides of a cylinder. Due to the challenge of directly manipulating and measuring the intensity of axial flow, Matsumoto et al. (2010) installed a perforated splitter plate in the wake center of a non-yawed circular cylinder in a wind tunnel study. By varying the perforation ratio

of the splitter plate, the intensity of von Kármán vortex shedding from the cylinder body can be controlled in a stationary state. Their results implied that the generation mechanism of dry inclined cable galloping might be associated with the suppression of the von Kármán vortex shedding.

Many researchers investigated the impact of placing a solid plate in the near wake of a cylinder on its surrounding flow structure. (Roshkot 1954) discovered that the base pressure of a circular cylinder would be substantially increased if a long solid splitter plate was present in the wake. Apelt et al. (1973) and Apelt and West (1975) conducted experiments by placing solid splitter plate of different lengths downstream of a circular cylinder. They concluded that the near wake structure of the cylinder might be studied in the absence of von Kármán vortex formation. A few other studies also discussed how the communication interruption between the separated shear layers in the wake region of a cylindrical body in the presence of a solid splitter plate would affect the aerodynamic forces acting on it (Ozono, 1999; Choi, 2007; Dehkordi and Jafari, 2010; Ali et al., 2012). On the other hand, experimental studies on the effect of a perforated/permeable wake splitter plate on the flow structure around a circular cylinder were rarely reported in literature. Cardell (1993) indicated that if a permeable splitter plate was placed in the wake of a cirucluar cylinder, both drag and von Kármán vortex shedding frequency would drop. In addition, provided the plate solidity was high enough, the base pressure of the cylinder was found to be independent of the Reynolds number and the plate solidity. As far as the numerical simulation is concerned, the solid wake splitter plate effect was investigated by a number of researchers in the relatively low Reynolds number regime (Kwon and Choi, 1996; Hwang et al., 2003, 2007; Vu et al., 2015); whereas to the best knowledge of the authors, reported numerical study on the flow structure around a circular cylinder with a perforated wake splitter plate is scarce.

Existing studies showed that the extent of communication between the separated shear

layers was critical to the characteristics of the cylinder wake. Abernathy and Kronauer (1962) proposed that, in the subcritical Reynolds number region, the von Kármán vortex street could form without a wake producing body, but rather by just bringing two shear layers of opposite sign within a communicable proximity of one another. Cardell (1993) confirmed the ability of permeable splitter plate in modifying the communication across the center plane of a circular cylinder wake. The effect of axial flow, on the other hand, on interrupting the communication between the two separated shear layers in the near wake region behind a circular cylinder was reported by Matsumoto et al. (2010). It was also suspected that the formation of axial vortex on the leeward side of the cylinder and the possible interaction between the axial vortex shedding and the conventional von Kármán vortex shedding in the wake could contribute to the aerodynamic instability of the cylinder. Their results indicated that galloping could be excited by introducing artificial axial flow in the near wake of a non-yawed circular cylinder. However, quite counter intuitively, it was also found that the velocity of axial flow, which might be related to the degree of interference on shear layer communication, had an inverse relation with the stability of the circular cylinder. Though the mechanism of axial flow on affecting the aerodynamic stability of a circular cylinder has not been fully unveiled, it is clear that part of its role is similar as that of the splitter plate, i.e. to interrupt the shear layer communication. Therefore, it is feasible to apprehend our understanding of the effect of axial flow, as well as its intensity, on the aerodynamic stability of a circular cylinder via placing a splitter plate with variable perforation ratio in its wake.

To unveil the possible relation between the von Kármán vortex shedding mitigation and the onset of dry inclined cable galloping, it is imperative to examine how change in the communication of separated shear layers would influence the flow structure around a circular cylinder and/or vice versa. In the current paper, a CFD simulation will be conducted to study flow past a non-yawed circular cylinder at a Reynolds number of 3900, with the presence of a perforated wake splitter plate. This particular

Reynolds number is selected mainly due to the availability of the existing experimental and numerical data, which can be used to validate the developed numerical model. By manipulating the solidity of the perforated wake splitter plate, the variation of von Kármán vortex shedding strength can be simulated. This would allow examining the impact of axial flow intensity on the aerodynamic behaviour of a circular cylinder indirectly and shed light on the role of axial flow in the excitation mechanism of dry inclined cable galloping.

## 2. NUMERICAL SIMULATION

### 2.1 Numerical approach

All simulations presented in this paper utilize the open source CFD Toolbox: OpenFOAM® V4.1 (Open Source Field Operation and Manipulation). The incompressible solver pisoFOAM uses a finite volume cell-centered discretization of the domain and handles unstructured mesh data format based on the so-called face-addressing storage using Pressure-Implicit with Splitting of Operators algorithm (PISO). Linear Green-Gauss is used for computing the gradient. The treatments of convective terms for velocity, kinematic turbulent energy, kinematic turbulent viscosity are Gauss LUST (blended 75% linear and 25% linearUpwind) and Gauss limitedLinear for the last two terms. A second-order accuracy scheme backward method is used for temporal discretization. A time step of $10^{-4}$ second is employed to guarantee the maximum Courant number to be smaller than 0.2 during the simulation. A geometric agglomerated algebraic multigrid solver (GAMG) with the Gauss-Seidel smooth method iteratively solves the linear algebraic system with a local accuracy of $10^{-6}$ for the pressure and $10^{-7}$ for the remaining variables at each time step.

The current study mainly focuses on the unsteady-state flow and hence the detailed instantaneous flow characteristics are critical to the investigation. In the Reynolds-averaged Navier-Stokes (RANS) approach, one only solves the averaged fluid field while the effect of all scales of instantaneous turbulent motion is modelled by a

turbulent model. The direct numerical simulation (DNS) directly solves the full Navier-Stokes equations using extremely fine spatial and temporal discretization to capture eddies at all scales in the given problems at a huge computational cost. The large eddy simulation (LES) is based on the filtered Navier-Stokes equations (Smagorinsky, 1963). Instead of adopting the conventional time averaging RANS approach with additional modelled transport equations, LES simulates eddies which are larger than the smallest grid size directly, while it treats the eddies under this scale by using the subgrid-scale (SGS) model with relatively lower computational resources than DNS. A novel approach of the hybrid LES-RANS method, i.e. the detached eddy simulation (DES), solves the attached portion of the boundary layers with the traditional RANS and uses LES in the separated flow regions. However, when using DES, the treatment of the boundary layer in the vicinity of the cylinder is not sufficient to unveil the properties of the highly unsteady flow. Therefore, the LES turbulent model is adopted in the current study to investigate the effect of a perforated wake splitter plate on the flow characteristics around a circular cylinder.

The governing equations, the Navier-Stokes equations, are based on the conservation laws for mass, momentum and energy. Since only the large eddies are directly computed in LES, so a low-pass spatial filter is applied to the Navier-Stokes equations. The filtered equations for a Newtonian incompressible flow can be written in a conservative form as:

$$\partial_i \overline{u}_i = 0 \tag{1}$$

$$\partial_t(\rho\overline{u}_i) + \partial_j\left(\rho\overline{u}_i\overline{u}_j\right) = -\partial_i\overline{p} + 2\partial_j\left(\mu\overline{S_{ij}}\right) - \partial_j(\tau_{ij}) \tag{2}$$

$$\overline{S_{ij}} = \frac{1}{2}(\partial_i\overline{u}_j + \partial_j\overline{u}_i) \tag{3}$$

$$\tau_{ij} = \frac{1}{2}(\overline{u_i u_j} - \overline{u}_i\overline{u}_j) \tag{4}$$

where $\rho$ is the density of the air, $\overline{u}_i$ is the filtered velocity, $\overline{p}$ is the filtered pressure, $\mu$ is the dynamics viscosity, $\overline{S_{ij}}$ is the filtered strain rate tensor, and $\tau_{ij}$ is the unknown SGS stress tensor, which represents the small scale motions. To solve the above

equations, the SGS eddy viscosity needs to be determined. The most basic model is the one originally proposed by Smagorinsky (1963), i.e.

$$\mu_t = \rho(C_s\overline{\Delta})^2 S \tag{5}$$

$$S = (2\overline{S}_{ij}\overline{S}_{ij})^{\frac{1}{2}} \tag{6}$$

$$\Delta = (\Delta x \Delta y \Delta z)^{\frac{1}{3}} \tag{7}$$

where $C_s$ is the Smagorinsky constant depending on the type of the flow.

### 2.2 Computational domain

The coordinate system, the definition of the angle $\theta$, which represents the angular position of an arbitrary point on the cylinder surface with respect to the stagnation point, and the span-wise length are shown in the Figure 1(a). Figure 1(b) illustrates a schematic view of the computational domain of a classic case of flow past a circular cylinder. The diameter of the studied circular cylinder is $D$ = 0.0889 m. The center of the cylinder coincides with the origin of the computational domain. From the origin, the computational domain extends $10D$ towards the inlet and $20D$ towards the outlet, and from -$10D$ to $10D$ in the cross-flow direction. The span-wise extension $L_z$ is chosen to be $\pi D/2$, which is found to be more efficient while maintaining an acceptable accuracy based on the mesh independence test.

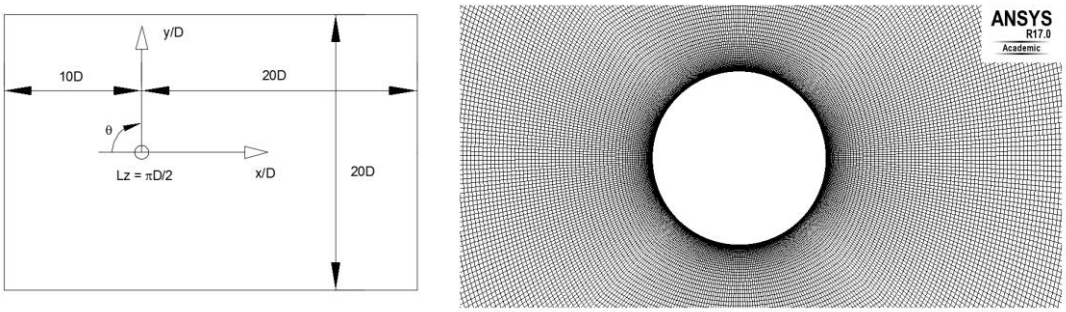


(a) Computational domain (b) Detailed grid in the near region of the circular cylinder

Fig. 1 Computational domain and detailed mesh for flow past a circular cylinder

ANSYS/ICEM is used to generate a block structured rectangular computational domain, as shown in Figure 1(b). The non-dimensional viscous length scale is defined as:

$$y^+ = (u_* \cdot y)/\nu \tag{8}$$

where $u_*$ is the friction velocity at the near wall, $y$ is the distance to the wall and $\nu$ is the local kinematic viscosity of the fluid. The height of the first cell on the cylinder is $9.57\times10^{-4}D$, which guarantees $y^+$ is smaller than 1. The no-slip condition is imposed on the surface of the cylinder and the plate. The span-wise resolution $\Delta z$ is $0.05D$ with 32 nodes along the z-axis. 392 nodes are employed on the cylinder surface along the circumference for the no wake splitter plate case. The total number of control volumes for the solid plate case is $5.57\times10^6$. A non-dimensional time step $\Delta t$ of $7.4\times10^{-4}$ is used, where $\Delta t = Ut/D$. A Dirichlet boundary condition for velocity ($u = 0.658\ m/s; v = 0; w = 0$) and a Neumann boundary condition for zero gradient pressure are prescribed at the inlet. A Dirichlet boundary condition for zero pressure is applied at the outlet. A cyclic boundary condition is employed on the span-wise walls.

When introducing a piece of splitter plate along the central line of a circular cylinder wake, not only the perforation ratio, but also the size and the position of the plate could have a sizable impact on the cylinder wake structure. (Roshkot 1954) found that a splitter plate of length $5D$ ($D$ is the cylinder diameter) inhibited the periodic formation of the von Kármán vortices, whereas it was not the case if the plate length was shortened to $1.14D$. Besides, Cardell (1993) investigated the influence of the gap size between the splitter plate and the cylinder on the flow properties around the cylinder. Results showed that if the gap was less than 0.13 $D$, the presence of the splitter plate would not have an appreciable effect on the cylinder mean base pressure and the von Kármán vortex shedding frequency. Based on these, to explore how the variation of the von Kármán vortex shedding strength would affect the flow structure around a circular cylinder, in the current numerical study, a wake splitter plate of length $D$ and thickness $D/20$ was placed along the central line of the cylinder wake

with a gap of 0.11 *D* between the cylinder and the plate.

Figure 2 shows a 3D view of the detailed mesh near the cylinder and the solid wake splitter plate. For the perforated plate, the perforation ratio is defined as the ratio between the opening length and the total length of the splitter plate along the flow direction. A total of four perforation ratio levels, i.e. 0, 1/3, 2/3, and 1, are simulated in the current study, of which a perforation ratio of 0 represents the solid splitter plate case, whereas 1 represents the no splitter plate case. The mesh details of the perforation ratio cases of 1/3 and 2/3 are given in Figures 3(a) and 3(b), respectively.

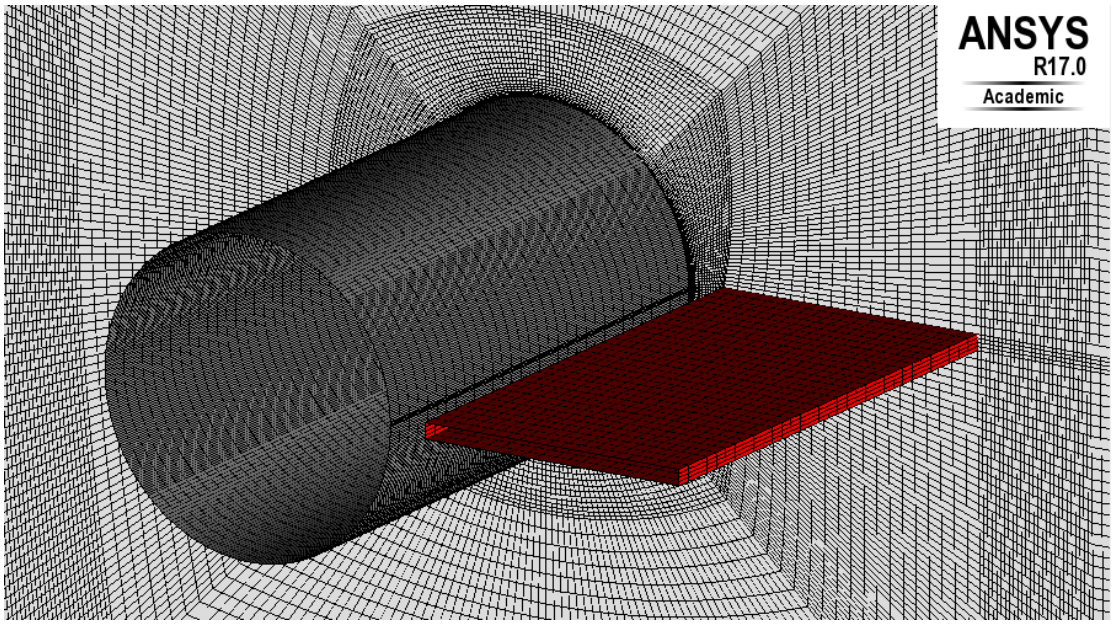


Fig. 2 Detailed mesh near the cylinder and the solid splitter plate (perforation ratio of 0)

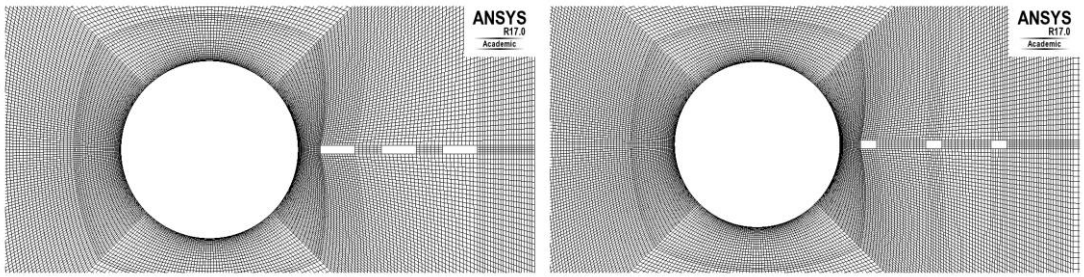


(a) Perforation ratio of 1/3 (b) Perforation ratio of 2/3

Fig. 3 Mesh details of the perforated wake splitter plate cases

Regarding the mesh generation scheme in the perforated splitter plate cases, the O-shape meshes were first introduced in the near region of the cylinder. Then, based on the studied perforation ratio, the block near the splitter plate region was further divided into 7 and 16 sub-blocks, with the quadrilateral meshes generated in each sub-block. Finally, the three-dimensional meshes were generated by extending the two-dimensional plane along the span-wise direction.

### 2.3 Model validation

The validity of the developed numerical model was examined using the no splitter plate case at a Reynolds number of 3900. Two different meshes, Mesh 1 and Mesh 2 were used for the model validation test. They had the same 2-dimensional grid, but the number of nodes in the span-wise direction was taken as 16 and 32, respectively. The span-wise resolution, i.e. the distance between the two adjacent span-wise nodes, was kept the same at $\pi D/64$. The drag coefficient and the Strouhal number of the circular cylinder obtained from these two meshes are listed in Table 1, along with the data reported in literature (Lourenco and Shih, 1993; Breuer, 1998; Kravchenko and Moin, 2000 Tremblay et al., 2002; Prsic et al., 2012). It can be seen from Table 1 that the Strouhal number obtained from the current numerical models, both Mesh 1 and Mesh 2, agree very well with those in the literature. In terms of the drag coefficient, though the results yielded from both meshes fall within the range documented in the existing studies, the relatively higher drag coefficient obtained from Mesh 1 suggests that the span-wise length used in Mesh 1 could be insufficient. By doubling the span-wise length in Mesh 2, the drag coefficient drops from 1.32 to 1.20 by 10% and has a better agreement with the literature data. Therefore, Mesh 2 is used in the rest of the study.

Table 1 Model validation results

| Model | Method | Number of vortex shedding periods | Number of control volume (million) | $C_d$ | $S_t$ |
|---|---|---|---|---|---|
| Mesh 1 | LES | 10 | 2.3 | 1.32 | 0.22 |
| Mesh 2 | LES | 10 | 5.5 | 1.20 | 0.21 |
| Lourenco and Shih (1993) | PIV | - | - | 0.99 | 0.22 |
| Breuer (1998) | LES | 22 | 0.87 to 1.74 | [0.97 - 1.49] | [0.21-0.22] |
| Kravchenko and Moin (2000) | LES | 7 | 0.5 to 2.4 | [1.04-1.36] | [0.19-0.21] |
| Tremblay et al. (2002) | LES | - | - | [1.14 - 1.31] | [0.21-0.22] |
| Prsic et al. (2012) | LES | 60 | 5 to 11 | [1.10 - 1.24] | 0.21 |

## 3 RESULTS AND DISCUSSIONS

### 3.1 Instantaneous vortex structure

Flow around a non-yawed circular cylinder with the presence of a perforated wake splitter plate is investigated numerically at a Reynolds number of 3900. The effect of axial flow on the flow structure around the cylinder is examined indirectly by placing a perforated splitter plate in the near wake of the cylinder. Since the strength of the von Kármán vortex shedding is dictated by the perforation ratio of the wake splitter plate, four different perforation ratios, i.e. 0 (solid splitter plate), $1/3$, $2/3$ and 1 (no splitter plate), are simulated in the current study to examine the impact of the axial flow intensity on the aerodynamic behaviour of a circular cylinder.

The Galilean-invariant vortex criterion is commonly used to investigate the vortex structure in LES. In this criterion, the velocity gradient $\boldsymbol{\nabla v}$ is decomposed into

$$\boldsymbol{\nabla v} = \boldsymbol{S} + \boldsymbol{\Omega} \tag{9}$$

where $\boldsymbol{S} = \frac{1}{2}\left[\boldsymbol{\nabla v} + (\boldsymbol{\nabla v})^T\right]$ is the rate-of-strain tensor, and $\boldsymbol{\Omega} = \frac{1}{2}\left[\boldsymbol{\nabla v} - (\boldsymbol{\nabla v})^T\right]$ is the vorticity tensor. The first three-dimensional vortex criterion using Eq. (9) is the *Q-criterion* by Hunt et al, (1988). The definition of $Q$ is given as

$$Q = \frac{1}{2}\left[|\boldsymbol{\Omega}|^2 - |\boldsymbol{S}|^2\right] \tag{10}$$

The $Q$ value of the isosurfaces is 300 ($s^{-2}$), and its contour range of the vorticity varies from -30 to 30 ($s^{-1}$). Figure 4 shows the span-wise component, $\omega_z$, of the instantaneous vorticity for the no splitter plate (perforation ratio = 1) and the solid splitter plate (perforation ratio = 0) cases. The span-wise vorticity component $\omega_z$ describes the formation structure of the two shear layers on both sides of the circular cylinder. The numerical simulation results in Figure 4 demonstrate that the presence of a solid splitter plate would change the cylinder near wake structure by interrupting the communications between the two separated shear layers and extend their development range in the wake. Thus, a wake splitter plate could have a similar role as the axial flow on the leeward side of the cylinder.

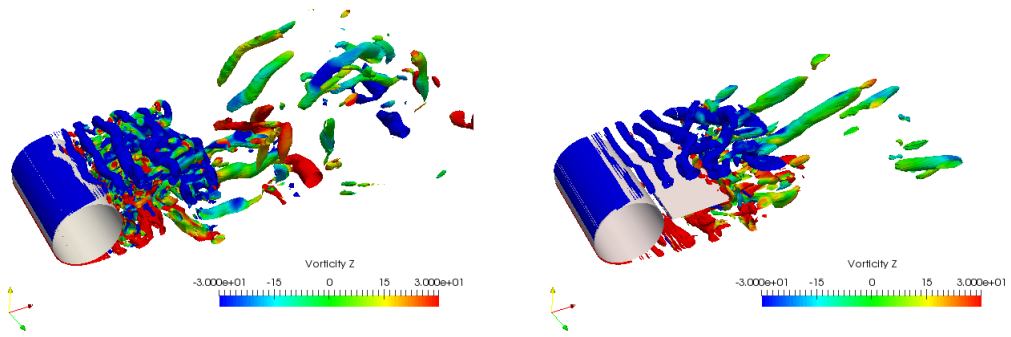


(a) Perforation ratio = 1 (no splitter plate) (b) Perforation ratio = 0 (solid splitter plate)

Fig. 4 Instantaneous vortex structures (Q =300 [$s^{-2}$])

The variations of the instantaneous vortex contour in the cylinder near wake at $z = D/4$ within one cycle of vortex shedding are illustrated in Figure 5 for the four perforation ratio cases. It can be observed from the figure that as the perforation ratio of the splitter plate decreases, the recirculation length gradually becomes longer. As a consequence, the near wake becomes more stable since the interaction between the two separated shear layers is more constrained. This clearly indicates that the intensity of von Kármán vortex shedding is controlled by the perforation ratio of the wake splitter plate.

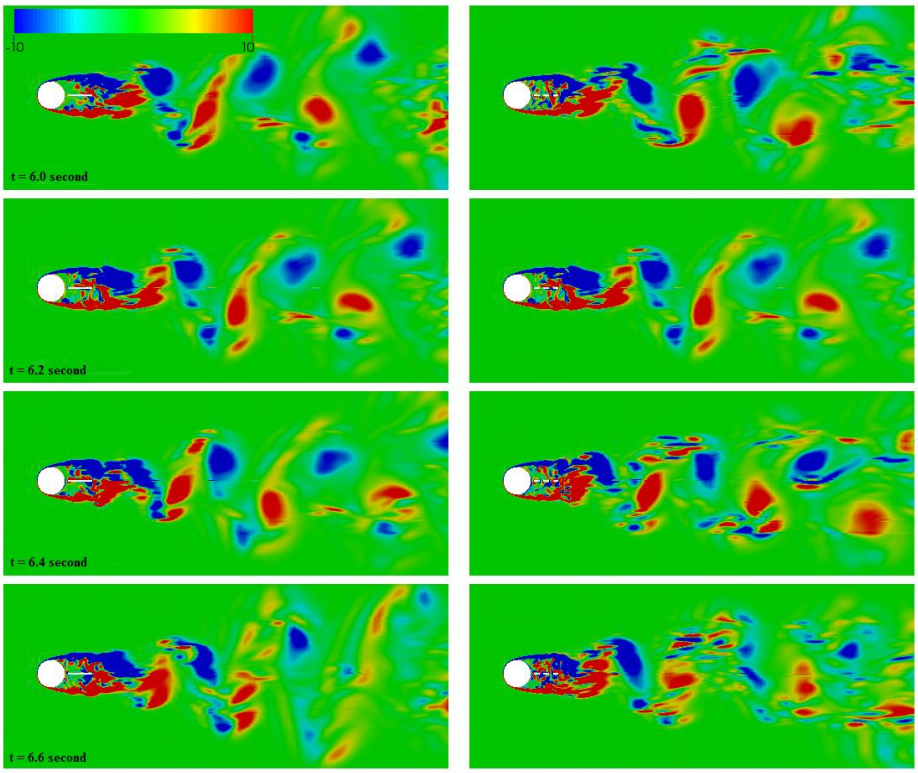


(a) Perforation ratio = 0 (solid splitter plate) (b) Perforation ratio = $1/3$

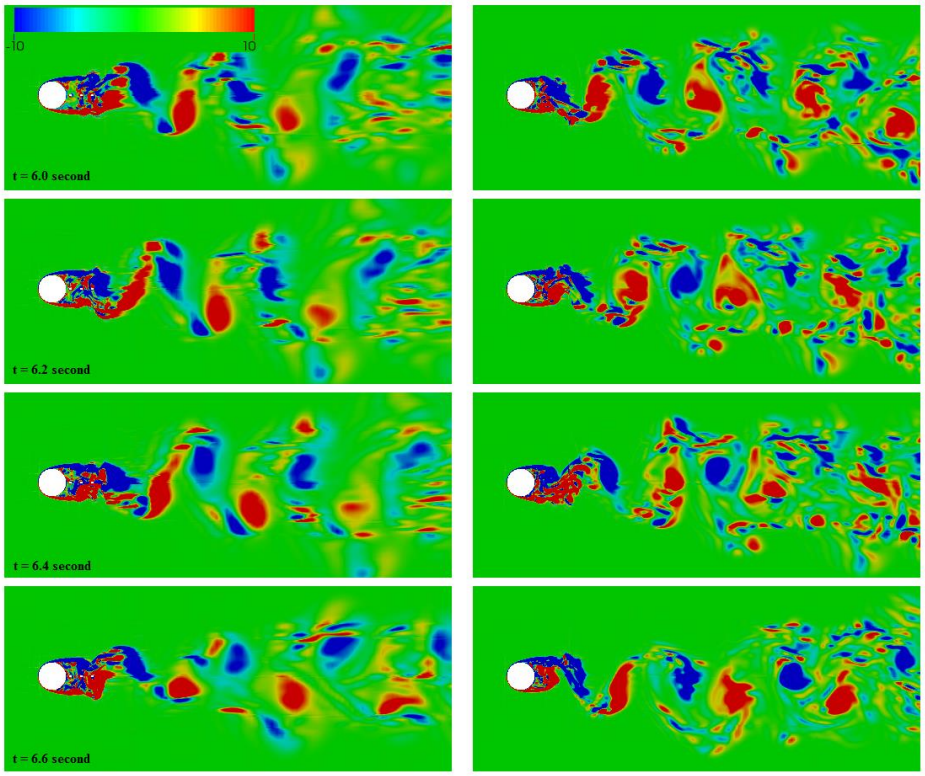


(c) Perforation ratio = 2/3 (d) Perforation ratio = 1 (no splitter plate)

Fig. 5 Instantaneous z-axis vortex contour (Q =300 [$s^{-2}$]) at mid-plane (z=D/4)

### 3.2 Surface pressure distribution

Figure 6 shows snap shots of the instantaneous surface pressure distribution along the circumference of the studied circular cylinder at its middle plane, in terms of the non-dimensional surface pressure coefficient $C_p$, for the four different perforation ratio cases at time instants of 6.0, 6.2, 6.4 and 6.6 second. They cover approximately a full period of von Kármán vortex shedding. It is worth mentioning that time instant 6.0 second is slightly lag behind that corresponding to zero instantaneous lift. The black solid line represents the cylinder surface. The non-dimensional surface pressure coefficient $C_p$ is defined as

$$C_p = \frac{p - p_0}{\rho U_\infty^2/2} \tag{11}$$

where $p$ is the instantaneous surface pressure of the cylinder, $p_0$ is the reference pressure at the infinite upstream, $\rho$ is the density of the fluid, and $U_\infty$ is the freestream velocity of the flow. As can be seen from Figure 6(a), when the splitter plate is solid,

i.e. the perforation ratio is 0, the instantaneous surface pressure distribution profiles at the four studied time instants within one vortex shedding period has no sizable difference and remain symmetric. With the decrease of the plate perforation ratio, the difference between them within approximately one vortex shedding period, though still small, increases gradually, as shown in Figures 6(b) and 6(c). When the splitter plate is removed from the wake (perforation ratio of 1), a clear variation of the instantaneous surface pressure distribution profile within approximately one vortex shedding period can be observed from Figure 6(d). In particular, the surface pressure distribution pattern becomes asymmetric at time instant 6.2 second, which is approximately at 1/4 of a vortex shedding period. This suggests that by placing a piece of more solid wake splitter plate, it would "stabilize" the variation of the instantaneous surface pressure distribution and alter the associated pattern to be more symmetric about the flow direction. Therefore, the strength of the von Kármán vortex shedding would be weakened. In addition, the base pressure of the cylinder is found to gradually increase with a more solid wake splitter plate.

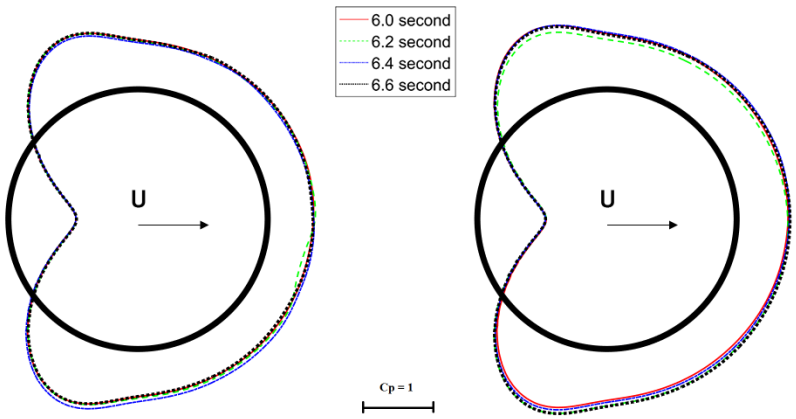


(a) Perforation ratio = 0 (b) Perforation ratio = 1/3

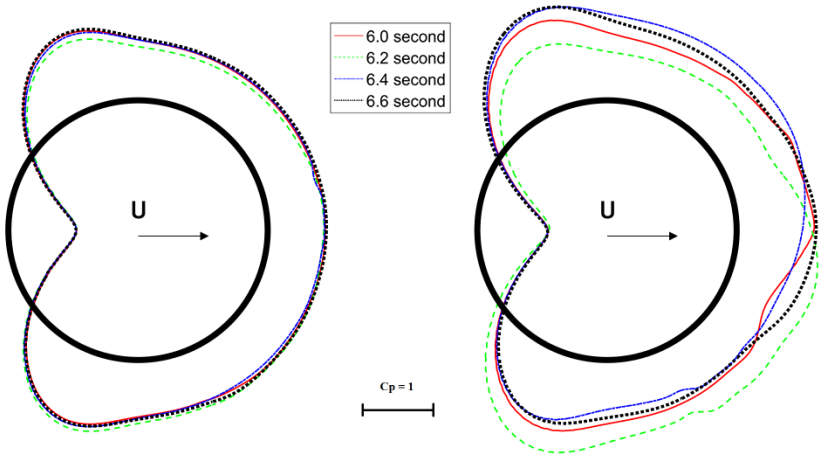


(c) Perforation ratio = $2/3$ (d) Perforation ratio = 1

Fig. 6 Instantaneous surface pressure distribution profile at cylinder mid-plane ($z = D/4$)

Figure 7 shows the influence of the wake splitter plate perforation ratio on the mean surface pressure coefficient distribution pattern of the circular cylinder. Similarly, it can be clearly seen from the figure that when no wake splitter plate is present (perforation ratio of 1), the distribution of the cylinder surface pressure is symmetric about the flow direction. With the gradual decrease of the perforation ratio, i.e. the wake splitter plate being more and more solid, the absolute value of the pressure coefficients gradually decrease, implying the strength of the von Kármán vortex shedding is weakened. In addition, it can be seen from Figure 7 that as the perforation ratio increases, the absolute value of the mean surface pressure coefficient would increase accordingly, except for the perforation ratio case $2/3$, of which the surface pressure at the bottom side of the cylinder is found to be slightly higher than the other cases. This could be associated with the time duration over which the mean surface pressure coefficient is computed. In the current study, it is calculated based on 10 von Kármán vortex shedding periods. Further, such a change in the plate perforation ratio would result in a decrease in the base pressure.

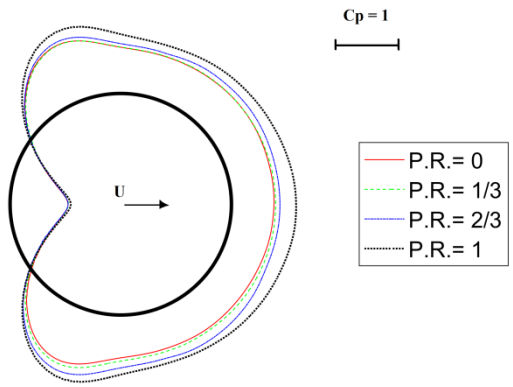


Fig. 7 Ten periods mean surface pressure distribution profile of the cylinder

In general, the results in Figures 6 and 7 indicate that the perforation ratio of the wake splitter plate would dictate the symmetry of the surface pressure distribution pattern around a circular cylinder and the magnitude of the base pressure, and thus affect the flow structure around the cylinder. The formation of axial flow on the leeward side of an inclined and/or yawed stay cable is suspected to play a similar role as the wake splitter plate in mitigating the strength of von Kármán vortex shedding, which would consequently affect the cable surface pressure distribution pattern and ultimately its wind-induced forces and responses.

### 3.3 Aerodynamic forces

When flow past a solid body, it would exert pressure forces normal to the body surface and shear forces tangent to it. The resultant force of these two is usually decomposed into an along-flow component, i.e. the drag force, and a cross-flow component, i.e. the lift force. For the Reynolds number 3900 scenario studied in the current paper, the viscous shear force can be neglected. Thus, the lift force and the drag force acting on the circular cylinder can be evaluated by integrating the normal pressure over the cylinder circumferential surface. The sectional lift and drag forces can be computed from

$$F_l = \int_0^{2\pi} p \cdot \overrightarrow{n_y} \cdot r \cdot d\theta = \sum_0^n p \cdot \overrightarrow{n_y} \cdot r \cdot \Delta\theta \tag{12}$$

$$F_d = \int_0^{2\pi} p \cdot \overrightarrow{n_x} \cdot r \cdot d\theta = \sum_0^n p \cdot \overrightarrow{n_x} \cdot r \cdot \Delta\theta \tag{13}$$

where $F_l$ and $F_d$ are respectively the sectional lift and drag forces, $p$ is the surface pressure at a specific point on the cylinder surface, $\overrightarrow{n_x}$ and $\overrightarrow{n_y}$ are respectively the wall normal vector in the *x*-and *y*-direction at that surface point, $r$ is the radius of the cylinder, $n$ is the total number of nodes along the cylinder circumference, which is 392 in the current study, and $\Delta\theta = 2\pi/n$. The non-dimensional form of the time $t$, the sectional lift force $F_l$, the sectional drag force $F_d$, and the von Kármán vortex shedding frequency $f$ are designated as $T^*$, $C_l$, $C_d$, and $S_t$ respectively. They are defined as follows:

$$T^* = T \cdot U_\infty / D \tag{14}$$

$$C_l = \frac{F_l}{\rho U_\infty^2/2} = \frac{1}{2}\sum_0^n C_p \cdot \overrightarrow{n_y} \cdot \Delta\theta \tag{15}$$

$$C_d = \frac{F_d}{\rho U_\infty^2/2} = \frac{1}{2}\sum_0^n C_p \cdot \overrightarrow{n_x} \cdot \Delta\theta \tag{16}$$

$$S_t = f \cdot D/U_\infty \tag{17}$$

where $C_p$ is the non-dimensional surface pressure coefficient defined by Eq. (11), $\rho$ is the density of the fluid, $U_\infty$ is the freestream velocity of the flow, $t$ is the dimensional time and $D$ is the cylinder diameter.

Figures 8 and 9 depict respectively the time history of the lift and drag coefficients over a time duration of approximately 10 vortex shedding periods for the four studied wake splitter plate perforation ratio cases. The mean drag coefficient, the root-mean-square and the maximum instantaneous lift coefficient, which are computed based on the simulated time history of 10 vortex shedding periods, are summarized in Table 2. In terms of the statistical convergence, the averaging time used for computing these statistics differ significantly from one to the other in the existing studies (Parnaudeau et al., 2008). For instance, (Kravchenko and Moin 2000) considered only 7 vortex

shedding periods, whereas Franke (2002) suggested to use 40 vortex shedding periods to obtain accurate mean flow in the neighborhood of a cylinder. In the case of Dong et al. (2006), 40-50 vortex shedding cycles were simulated. However, Parnaudeau et al., (2008) observed that the convergence level of a given set of data is very delicate to evaluate. They could compute a set of first and second order statistics in excellent agreement with their experimental data based on a simulated time history of 12 vortex shedding periods instead of 52 periods. In the current study, it is found that the mean drag coefficient of 1.2054 computed based on a time history of 10 vortex shedding periods does not differentiate too much from that based on a time history of 30 vortex shedding periods, which is 1.2436. Therefore, the current results will be based on a simulated time history of 10 vortex shedding periods.

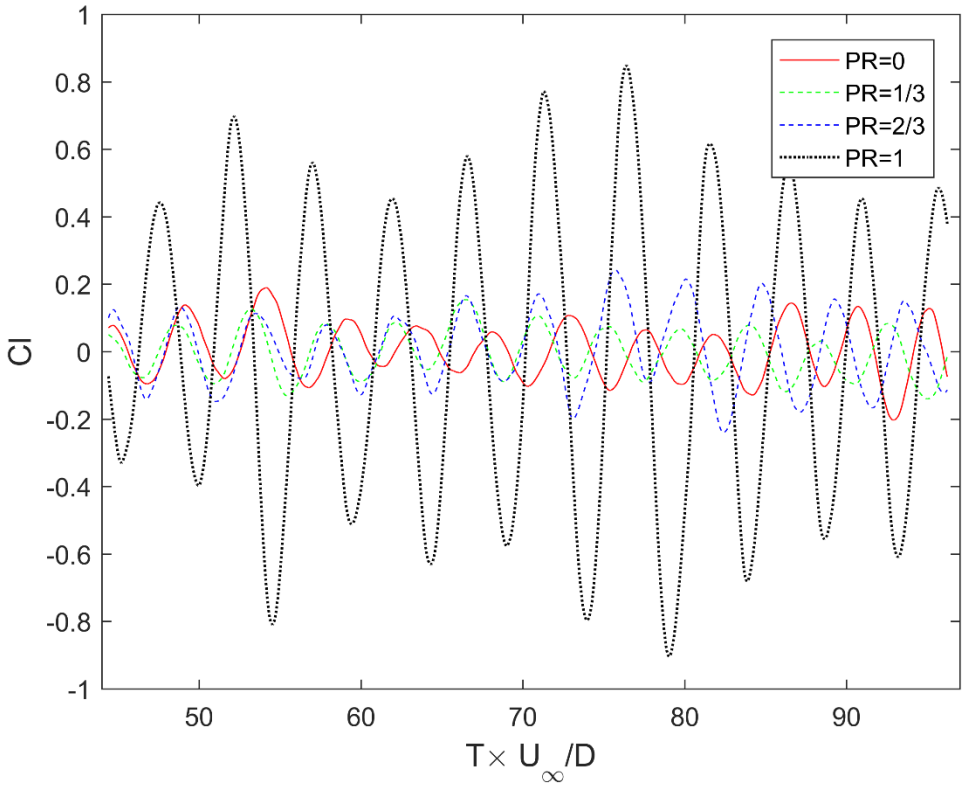


Fig. 8 Lift coefficient time histories for the four wake splitter plate perforation ratio cases

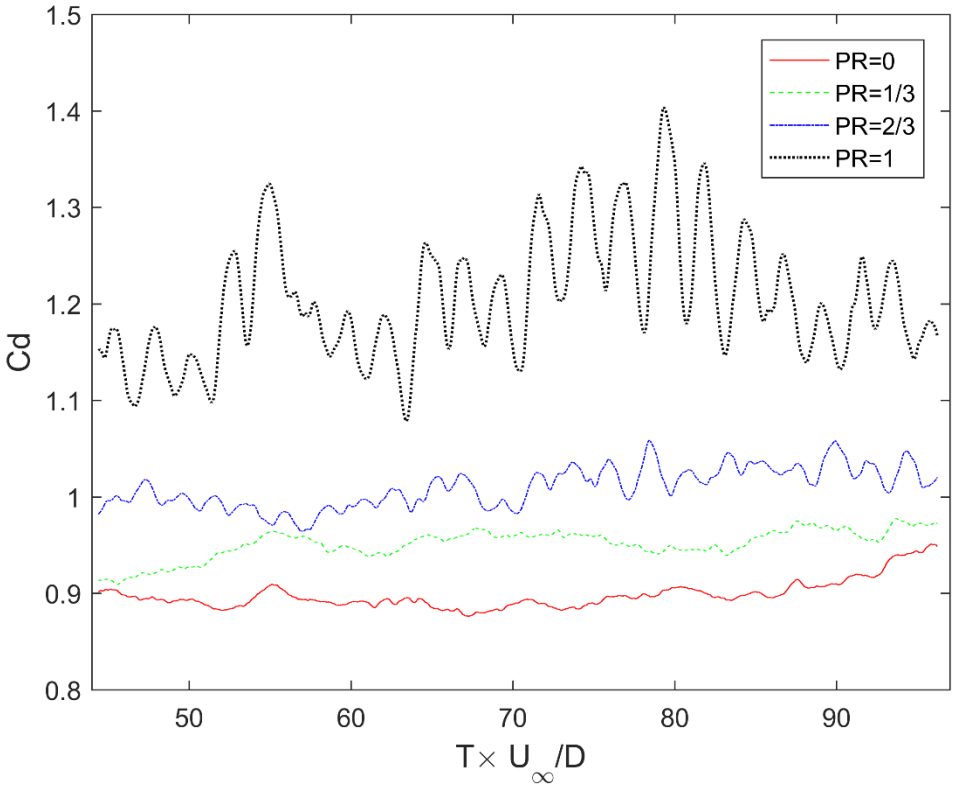


Fig. 9 Drag coefficient time histories for the four wake splitter plate perforation ratio cases

Table 2 Summary of the aerodynamic force coefficients

| Force coefficient | Perforation ratio | | | |
|---|---|---|---|---|
| | 0 | 1/3 | 2/3 | 1 |
| $C_{d,mean}$ | 0.90 | 0.95 | 1.01 | 1.20 |
| $C_{l,rms}$ | 0.08 | 0.07 | 0.10 | 0.44 |
| $C_{l,max}$ | 0.19 | 0.15 | 0.24 | 0.84 |

The lift coefficient time histories depicted in Figure 8 show that the fluctuation amplitude of the instantaneous lift is significantly affected by the presence of a perforated wake splitter plate. As given in Table 2, by decreasing the plate perforation ratio from 1 (no plate) to 0 (solid plate), the maximum instantaneous lift coefficient would reduce from 0.84 to 0.19 by 4.4 times, whereas the root-mean-square of the lift coefficient would drop more than 5 times from 0.44 to 0.08. This set of results indicates that a more solid wake splitter plate would discourage the shedding of the von Kármán vortex in the wake.

The mean drag results in Table 2 and the drag coefficient time histories in Figure 9 indicate that the presence of a wake splitter plate would decrease the drag on a circular cylinder. This reduction effect becomes more considerable should the perforation ratio of the plate gradually decrease, i.e. the plate being more and more solid. The same phenomenon was reported in the literature by Apelt et al. (1973) who used a solid wake splitter plate, and Cardell (1993) who used a permeable wake splitter plate having a solidity of 0.65. The latter is close to the current case of perforation ratio 1/3. Cardell (1993) conducted an experimental study at Reynolds number 4800 and found that compared to the no-plate case, the installation of a permeable wake splitter plate of solidity 0.65 caused a reduction in the cylinder mean drag coefficient from 1.00 to 0.76 by 24%. Whereas in the current simulation, a mean drag coefficient of 1.20 and 0.95 was obtained respectively for the no-plate and the perforation ratio 1/3 cases at Reynolds number 3900, which leads to a drag reduction of 21%. Further, the pattern of the four drag coefficients time history curves in Figure 9 suggests that the fluctuation of the instantaneous drag is mitigated by the existence of a wake splitter plate, and the suppression effect is enhanced with the decrease of perforation ratio. This implies that the installation of a more solid wake splitter plate would result in a stronger interruption in the communications between two separated shear layers.

## 4 CONCLUSIONS

Vulnerability of bridge stay cables to dynamic excitations like wind is one of the contemporary challenges in the design of modern cable-stayed bridges. Though dry inclined cable galloping has only been observed in a few wind tunnel tests so far, its possible occurrence on site should not be disregarded due to its significant consequence. Research effort in the past two decades identified a number of factors that could possibly contribute to the generation mechanism of this type of aerodynamic instability, and the presence of axial flow on the leeward side of the cable surface, which is resulted from the inclined and/or yawed orientation of a stay

cable against the oncoming wind, is one of them. It was speculated by some researcher that the onset of dry inclined cable galloping could be associated with the mitigation of von Kármán vortex shedding in the presence of axial flow, the intensity of which would directly affect the strength of von Kármán vortex shedding. To better understand the role of axial flow in exciting dry inclined cable galloping, how the change in axial flow intensity, or in other words, the strength of von Kármán vortex shedding in the wake, would influence the flow structure around a stay cable needs to be fully explored.

A numerical simulation has been conducted in the current paper to study flow past a non-yawed circular cylinder at a Reynolds number of 3900, with the presence of a perforated wake splitter plate. The strength of von Kármán vortex shedding is simulated by manipulating the perforation ratio of the perforated wake splitter plate. A total of four different perforation ratios of 0, 1/3, 2/3, and 1 have been considered in the current study. Results show that the change in the von Kármán vortex shedding strength could have a sizable impact on the flow structure around a circular cylinder and the aerodynamic forces acting on it. With the gradual decrease of the plate perforation ratio, i.e. the presence of a more solid wake splitter plate, a stronger interruption on the interaction between the shear layers formed on the two sides of the cylinder is observed, which subsequently alters the surface pressure distribution pattern to be more symmetric about the oncoming flow and reduces the strength of von Kármán vortex shedding in the wake. Such a change in the surrounding flow structure results in a decrease in the fluctuating amplitude of the instantaneous lift and drag acting on the cylinder and also the mean drag, which would ultimately affect the flow-induced responses of the cylinder. On site, if the combination of the oncoming wind speed and cable orientation intensifies the axial flow strength to a certain level, it could possibly mitigate von Kármán vortex shedding and therefore influence the wind-induced forces acting on the stay cable and thus its aerodynamic responses. In the next phase of the study, the numerical simulation will be extended to higher

Reynolds number close to and within the critical regime to further explore how weakening in the von Kármán vortex shedding would trigger the onset of galloping instability on a stay cable.

**Acknowledgments**

The authors are grateful to Natural Sciences and Engineering Research Council of Canada (NSERC) for supporting this project. This work was made possible by supercomputer mp2 from Université de Sherbrooke, managed by Calcul Québec and Compute Canada, the operation of this supercomputer is funded by the Canada Foundation for Innovation (CFI), the ministère de l'Économie, de la science et de l'innovation du Québec (MESI) and the Fonds de recherche du Québec - Nature et technologies (FRQ-NT). The computational support by the visualization systems vdi-ferdora20 managed by Shared Hierarchical Academic Research Computing Network (SHARCNET: www.sharcnet.ca) is greatly acknowledged.

**References**

Abernathy, F. H., and Kronauer, R. E., 1962. "The Formation of Vortex Streets." *Journal of Fluid Mechanics* 13 (1): 1. doi:10.1017/S0022112062000452.

Alam, M. M. and Zhou, Y., 2007. "Turbulent Wake of an Inclined Cylinder with Water Running." *Journal of Fluid Mechanics* 589: 261–303. doi:10.1017/S0022112007007720.

Ali, M. S. M., Doolan, C. J., and Wheatley, V., 2012. "Low Reynolds Number Flow over a Square Cylinder with a Detached Flat Plate." *International Journal of Heat and Fluid Flow* 36: 133–41. doi:10.1016/j.ijheatfluidflow.2012.03.011.

Apelt, C. J., West, G. S., and Szewczyk, A. A., 1973. "The Effects of Wake Splitter Plates on the Flow Past a Circular Cylinder in the Range $10^4$<R<$5\times10^4$." *Journal of Fluid Mechanics* 61 (1). Cambridge University Press: 187. doi:10.1017/S0022112073000649.

Apelt, C. J. and West, G. S., 1975. "The Effects of Wake Splitter Plates on Bluff-Body Flow in the Range $10^4$<R<$5\times10^4$. Part 2." *Journal of Fluid Mechanics* 71 (1). Cambridge University Press:

1160–1445. doi:10.1017/S0022112075002479.

Bi, J., Wang, J., Shao, Q., Lu, P., Guan, J., and Li, Q., 2013. “2D Numerical Analysis on Evolution of Water Film and Cable Vibration Response Subject to Wind and Rain.” *Journal of Wind Engineering and Industrial Aerodynamics* 121: 49–59. doi:10.1016/j.jweia.2013.07.018.

Bosdogianni, A. and Olivari, D., 1996. “Wind- and Rain-Induced Oscillations of Cables of Stayed Bridges.” *Journal of Wind Engineering and Industrial Aerodynamics* 64 (96): 171–85. doi:10.1016/S0167-6105(96)00089-X.

Breuer, M., 1998. “Large Eddy Simulation of the Subcritical Flow Past a Circular Cylinder : Numerical and Modeling Aspects.” *International Journal for Numerical Methods in Fluids* 28 (9): 1281–1302. doi:10.1002/(SICI)1097-0363(19981215)28.

Cao, D., Tucker, R. W., and Wang, C., 2003. “A Stochastic Approach to Cable Dynamics with Moving Rivulets.” *Journal of Sound and Vibration* 268 (2): 291–304. doi:10.1016/S0022-460X(03)00205-0.

Cardell, G. S., 1993. “Flow Past a Circular Cylinder with a Permeable Wake Splitter Plate.” *Phd Thesis*.

Cheng, S., Larose, G. L., Savage, M. G., Tanaka, H. and Irwin, P. A., 2008a. “Experimental Study on the Wind-Induced Vibration of a Dry Inclined Cable-Part I: Phenomena.” *Journal of Wind Engineering and Industrial Aerodynamics* 96 (12): 2231–53. doi:10.1016/j.jweia.2008.01.008.

Cheng, S., Irwin, P., and Tanaka, H., 2008b. “Experimental Study on the Wind-Induced Vibration of a Dry Inclined Cable-PartPart II: Proposed Mechanisms.” *Journal of Wind Engineering and Industrial Aerodynamics* 96 (12): 2231–53. doi:10.1016/j.jweia.2008.01.008.

Cheng, S., Tanaka, H. 2005. " Correlation of aerodynamic forces on an inclined circular cylinder." Wind & Structures 8.2 135-146.

Cheng, S., Larose, G. L., Savage, M. G., and Tanaka, H., 2003. “Aerodynamic Instability of Inclined Cables.” In *Proceedings of the 5th International Symposium on Cable Dynamics*, 69–76.

Choi, H., 2007. “Control of flow Over a Bluff Body.” *Fifth International Symposium on Turbulence and Shear Flow Phenomena*. Begel House Inc.

Dehkordi, B. G. and Jafari, H. H., 2010. “On the Suppression of Vortex Shedding From Circular Cylinders Using Detached Short Splitter-Plates.” *Journal of Fluids Engineering* 132 (4). American Society of Mechanical Engineers: 44501. doi:10.1115/1.4001384.

Dong, S., Karniadakis, G. E., Ekmekcia, A. and Rockwell, D., 2006. “A Combined Direct Numerical Simulation–particle Image Velocimetry Study of the Turbulent near Wake.” *Journal of Fluid Mechanics* 569: 185–207. doi:doi:10.1017/S0022112006002606.

Flamand, O., 1995. “Rain-Wind Induced Vibration of Cables.” *Journal of Wind Engineering and Industrial Aerodynamics* 57 (2–3): 353–62. doi:10.1016/0167-6105(94)00113-R.

Franke, J., 2002. “Large Eddy Simulation of the Flow Past a Circular Cylinder at Re=3900.” *Journal of Wind Engineering and Industrial Aerodynamics* 90: 1191–1206. doi:10.1016/S0167-6105(02)00232-5.

Gu, M. and Du, Q., 2005. “Testing Investigation for Rain-Wind Induced Vibration and Its Control of Cables of Cable-Stayed Bridges.” *J. of Wind Eng. & Indust. Aerodyn* 93 (1): 79595.

Gu, M. and Lu, Q., 2001. “Theoretical Analysis of Wind-Rain Induced Vibration of Cables of Cable-Stayed Bridges.” *APCWE-5, J. Wind Eng. Ind. Aerodynamic* 89: 125–28.

He, M. and Macdonald, J. H. G., 2016. “An Analytical Solution for the Galloping Stability of a 3 Degree-of-Freedom System Based on Quasi-Steady Theory.” *Journal of Fluids and Structures* 60. Elsevier: 23–36. doi:10.1016/j.jfluidstructs.2015.10.004.

He, X., Yu, X., and Chen, Z., 2012. “Nonstationarity Analysis in Wind-Rain-Induced Vibration of Stay Cables.” *Journal of Civil Engineering and Management* 18 (6): 821–27. doi:10.3846/13923730.2012.720933.

He, X., Fang, J., Scanlon, A., and Chen, Z., 2010. “Wavelet-Based Nonstationary Wind Speed Model in Dongting Lake Cable-Stayed Bridge.” *Engineering* 2 (11): 895–903. doi:10.4236/eng.2010.211113.

Hikami, Y. and Shiraishi, N., 1988. “Rain-Wind Induced Vibrations of Cables Stayed Bridges.” *Journal of Wind Engineering and Industrial Aerodynamics* 29 (1). Elsevier: 409–18. doi:10.1016/0167-6105(88)90179-1.

Hunt, J. C. R., Wray, A., and Moin, P., 1988. “Eddies, Streams, and Convergence Zones in Turbulent Flows.” *Center for Turbulence Research, Proceedings of the Summer Program*, no. 1970: 193–208. doi:CTR-S88.

Hwang, J. and Yang, K., 2007. “Drag Reduction on a Circular Cylinder Using Dual Detached Splitter Plates.” *Journal of Wind Engineering and Industrial Aerodynamics* 95 (7). Elsevier: 551–64.

Hwang, J., Yang, K., and Sun, S., 2003. “Reduction of Flow-Induced Forces on a Circular Cylinder

Using a Detached Splitter Plate." *Physics of Fluids* 15 (8). AIP: 2433–36.

Jakobsen, J. B., Andersen, T. L., Macdonald, J. H., Nikitas, G. N., Larose, G. L., Savage M. G., and McAuliffe, B. R., 2012. "Wind-Induced Response and Excitation Characteristics of an Inclined Cable Model in the Critical Reynolds Number Range." *Journal of Wind Engineering and Industrial Aerodynamics* 110. Elsevier: 100–112. doi:10.1016/j.jweia.2012.04.025.

Jing, H., Xia, Y., Li, H., Li, Y., and Xu, Y., 2017. "Excitation Mechanism of Rain-Wind Induced Cable Vibration in a Wind Tunnel." *Journal of Fluids and Structures* 68 (November 2015). Elsevier: 32–47. doi:10.1016/j.jfluidstructs.2016.10.006.

Kravchenko, A. G. and Moin, P., 2000. "Numerical Studies of Flow over a Circular Cylinder at {R}e= 3900." *Physics of Fluids* 12 (3900): 403–17. doi:10.1063/1.870318.

Kwon, K. and Choi, H., 1996. "Control of Laminar Vortex Shedding behind a Circular Cylinder Using Splitter Plates." *Physics of Fluids* 8 (2). AIP: 479–86.

Li, H., Chen,W., Xu, F., Li, F., and Ou, J., 2010. "A Numerical and Experimental Hybrid Approach for the Investigation of Aerodynamic Forces on Stay Cables Suffering from Rain-Wind Induced Vibration." *Journal of Fluids and Structures* 26 (7–8). Elsevier: 1195–1215. doi:10.1016/j.jfluidstructs.2010.06.006.

Li, S., Chen, Z., Asce, M., Sun, W., and Li, S., 2016. "Experimental Investigation on Quasi-Steady and Unsteady Self-Excited Aerodynamic Forces on Cable and Rivulet" 142 (1): 1–11. doi:10.1061/(ASCE)EM.1943-7889.0000961.

Li, S., Chen, Z., Asce, M., Wu, T., Asce, S., Kareem, M. A., Asce, D. M., et al., 2013. "Influence of Dynamic Properties and Position of Rivulet on Rain – Wind-Induced Vibration of Stay Cables" 139 (October): 1688–98. doi:10.1061/(ASCE)EM.1943-7889.0000612.

Lourenco, L. M. and Shih, C., 1993. "Characteristics of the Plane Turbulent near Wake of a Circular Cylinder, a Particle Image Velocimetry Study." *Private Communication*.

Macdonald, J. H. G. and Larose, G. L., 2008. "Two-Degree-of-Freedom Inclined Cable Galloping-Part 1: General Formulation and Solution for Perfectly Tuned System." *Journal of Wind Engineering and Industrial Aerodynamics* 96 (3): 291–307. doi:10.1016/j.jweia.2007.07.002.

Macdonald, J. H. G. and Larose, G. L., 2006. "A Unified Approach to Aerodynamic Damping and Drag/lift Instabilities, and Its Application to Dry Inclined Cable Galloping." *Journal of Fluids and Structures* 22 (2): 229–52. doi:10.1016/j.jfluidstructs.2005.10.002.

Main, J. A. and Jones, N. P., 2000. “A Comparison of Full-Scale Measurements of Stay Cable Vibration.” In *Proceedings of Structures Congress 2000*.

Matsumoto, M., Shiraishi, N., Kitazawa, M., Knisely, C., Shirato, H., Kim,Y., and Tsujii, M., 1990. “Aerodynamic Behavior of Inclined Circular Cylinders-Cable Aerodynamics.” *Journal of Wind Engineering and Industrial Aerodynamics* 33 (1). Elsevier: 63–72. doi:10.1016/0167-6105(90)90021-4.

Matsumoto, M., Shiraishi, N., and Shirato, H., 1992. “Rain-Wind Induced Vibration of Cables of Cable-Stayed Bridges.” *Journal of Wind Engineering and Industrial Aerodynamics* 43 (1). Elsevier: 2011–22. doi:10.1016/0167-6105(92)90628-N.

Matsumoto, M., Saitoh, T., Kitazawa, M., Shirato, H., and Nishizaki, T., 1995. “Response Characteristics of Rain-Wind Induced Vibration of Stay-Cables of Cable-Stayed Bridges.” *Journal of Wind Engineering and Industrial Aerodynamics* 57 (2–3): 323–33. doi:10.1016/0167-6105(95)00010-O.

Matsumoto, M., Shirato, H., Yagi, T., Goto, M., Sakai, S., and Ohya, J., 2003. “Field Observation of the Full-Scale Wind-Induced Cable Vibration.” *Journal of Wind Engineering and Industrial Aerodynamics* 91 (1–2): 13–26. doi:10.1016/S0167-6105(02)00332-X.

Matsumoto, M., Yagi, T., Hatsuda, H., Shima, T., Tanaka, M., and Naito, H., 2010. “Dry Galloping Characteristics and Its Mechanism of Inclined/yawed Cables.” *Journal of Wind Engineering and Industrial Aerodynamics* 98 (6–7). Elsevier: 317–27. doi:10.1016/j.jweia.2009.12.001.

Matsumoto, M., Yagi, T., Liu, Q., Oishi, T., and Adachi, Y., 2005. “Effects of Axial Flow and Karman Vortex Interference on Dry-State Galloping of Inclined Stay-Cables.” In *Proceedings of the 6th International Symposium on Cable Dynamics*, 247–54.

Ming, G. U., 2002. “Response Characteristic of Wind Excited Cables With Artificial Rivulet 23 (10): 1176–87.

Miyata, T., Yamada, H., and Hojo, T., 1994. “Aerodynamic Response of PE Stay Cables with Pattern-Indented Surface.” In *Proceedings of the International Conference on Cablestayed and Suspension Bridges (AFPC)*, 515–22.

Ozono, S., 1999. “Flow Control of Vortex Shedding by a Short Splitter Plate Asymmetrically Arranged Downstream of a Cylinder.” *Physics of Fluids* 11 (10): 2928–34. doi:10.1063/1.870151.

Pacheco, B. M., 1993. “Keeping Cables Calm.” *Civil Engineering—ASCE* 63 (10): 56–58.

Parnaudeau, P., Heitz, J. D., and Lamballais, E., 2008. “Experimental and Numerical Studies of the Flow over a Circular Cylinder at Reynolds Number 3900.” *Physics of Fluids* 20 (8). doi:10.1063/1.2957018.

Persoon, A. J. and Noorlander, K., 1999. *Full-Scale Measurements on the Erasmus Bridge after Rain/wind Induced Cable Vibrations*. Nationaal Lucht-en Ruimtevaartlaboratorium.

Piccardo, G., 1993. “A Methodology for the Study of Coupled Aeroelastic Phenomena.” *Journal of Wind Engineering and Industrial Aerodynamics* 48 (2). Elsevier: 241–52. doi:10.1016/0167-6105(93)90139-F.

Prsic, M., Ong, M. C., Pettersen, B., and Myrhaug, D., 2012. “Large Eddy Simulations of Three-Dimensional Flow Around a Pipeline in a Uniform Current.” In *ASME 2012 31st International Conference on Ocean, Offshore and Arctic Engineering*, 539–48.

Raeesi, A., Cheng, S., and Ting, D. S., 2014. “A Two-Degree-of-Freedom Aeroelastic Model for the Vibration of Dry Cylindrical Body along Unsteady Air Flow and Its Application to Aerodynamic Response of Dry Inclined Cables.” *Journal of Wind Engineering and Industrial Aerodynamics* 130. Elsevier: 108–24. doi:10.1016/j.jweia.2014.04.007.

Robertson, A. C., Taylor, I. J., Wilson, S. K., Duffy, B. R., and Sullivan, J. M., 2010. “Numerical Simulation of Rivulet Evolution on a Horizontal Cable Subject to an External Aerodynamic Field.” *Journal of Fluids and Structures* 26 (1). Elsevier: 50–73. doi:10.1016/j.jfluidstructs.2009.09.003.

Roshkot, A., 1954. “On the Drag and Shedding Frequency of Two-Dimensional Bluff Bodies.” *National Advisory Committee on Aeronautics*.

Saito, T., Matsumoto, M., and Kitazawa, M., 1994. “Rain-Wind Excitation of Cables on Cable-Stayed Higashi-Kobe Bridge and Cable Vibration Control.” In *Proceedings of the International Conference on Cable-Stayed and Suspension Bridges (AFPC)*, 2:507–10.

Seidel, C. and Dinkler, D., 2006. “Rain-Wind Induced Vibrations - Phenomenology, Mechanical Modelling and Numerical Analysis.” *Computers and Structures* 84 (24–25): 1584–95. doi:10.1016/j.compstruc.2006.01.033.

Shirakashi, M., Hasegawa, A., and Wakiya, S., 1986. “Effect of the Secondary Flow on Kármán Vortex Shedding from a Yawed Cylinder.” *Bulletin of JSME*.

Smagorinsky, J., 1963. “General Circulation Experiments With the Primitive Equations.” *Monthly*

*Weather Review* 91 (3): 99–164. doi:10.1175/1520-0493(1963)091<0099:GCEWTP>2.3.CO;2.

Stafford, D. G. and Watson, S. C., 1988. "Cables in Trouble." *Civil Engineering*.

Tremblay, F., Manhart, M., and Friedrich, R., 2002. "LES of Flow around a Circular Cylinder at a Subcritical Reynolds Number with Cartesian Grids." In *Advances in LES of Complex Flows*, 133–50. Springer.

Vo, H. D., Katsuchi, H., Yamada, H., and Nishio, M., 2016. "A Wind Tunnel Study on Control Methods for Cable Dry-Galloping." *Frontiers of Structural and Civil Engineering* 10 (1): 72–80. doi:10.1007/s11709-015-0309-7.

Vu, H. C., Ahn, J., and Hwang, J. H., 2015. "Numerical Investigation of Flow around Circular Cylinder with Splitter Plate." *KSCE Journal of Civil Engineering* 0 (0): 1–10. doi:10.1007/s12205-015-0209-3.

Wang, J., Lu, P., Bi, J., Guan, H. J., and Qiao, H. Y., 2016. "Three-Phase Coupled Modelling Research on Rain – Wind Induced Vibration of Stay Cable Based on Lubrication Theory" 63: 16–39.

Yamaguchi, H., 1990. "Analytical Study on Growth Mechanism of Rain Vibration of Cables." *Journal of Wind Engineering and Industrial Aerodynamics* 33 (1). Elsevier: 73–80. doi:10.1016/0167-6105(90)90022-5.

Zuo, D., Jones, N. P., and Main, J. A., 2008. "Field Observation of Vortex- and Rain-Wind-Induced Stay-Cable Vibrations in a Three-Dimensional Environment." *Journal of Wind Engineering and Industrial Aerodynamics* 96 (6–7): 1124–33. doi:10.1016/j.jweia.2007.06.046.

Zuo, D. and Jones, N. P., 2010. "Interpretation of Field Observations of Wind- and Rain-Wind-Induced Stay Cable Vibrations." *Journal of Wind Engineering and Industrial Aerodynamics* 98 (2). Elsevier: 73–87. doi:10.1016/j.jweia.2009.09.004.

Zuo, D. and Jones, N. P., 2009. "Wind Tunnel Testing of Yawed and Inclined Circular Cylinders in the Context of Field Observations of Stay-Cable Vibrations." *Journal of Wind Engineering and Industrial Aerodynamics* 97 (5–6). Elsevier: 219–27. doi:10.1016/j.jweia.2009.06.009.